**Proceedings of the ASME 2024
International Design Engineering Technical Conferences and
Computers and Information in Engineering Conference
IDETC/CIE2024
August 25–28, 2024, Washington, DC**

IDETC/CIE2024-143935

INTUITIVE PHYSICS-DRIVEN APPROACH: DESIGN AND CALIBRATION OF A FLIGHT CONTROLLER FOR INDOOR BLIMPS

Jorge Esteban Salas Gordoniz[1,*], Maarouf Saad[1], David St-Onge[1]

[1]École de Technologie Supérieure, Montreal, QC, Canada

ABSTRACT

This research addresses the challenges of defining and tuning a flight controller for uncrewed aerial vehicles (UAVs), mainly, a lighter-than-air vehicle, like a blimp; a task often fraught with complexity for UAV designers. These challenges typically involve several iterations in both simulation and real-world settings that require the identification of the dynamic model. In this paper, we introduce a novel, but simple approach that harnesses intuitive physics principles to streamline the process of tuning and to ensure the safeness and robust path tracking for indoor blimps. Our method involves a threefold strategy: 1. A basic control rooted in Sliding Mode Control (SMC) with a saturation term that permits to achieve the motion in the three axes (X, Y and Z), while defining maximum cruising speeds and maximum desired control forces; used to complete the operation of path tracking and hovering. 2. A recursive simple moving average (SMA) term for the applied control forces is incorporated to the previous strategy to minimize steady-state error in real-time for altitude control, which can compensate for changes in the weight of the blimp. 3. A swing stabilizer mechanism designed to dampen oscillations around naturally occurred pitch and roll angles for enhanced stability. Experimental results validate the efficacy and simplicity of our approach, demonstrating robustness, rapid deployment and good path accuracy.

Keywords: Control, tuning, blimps.

NOMENCLATURE

m	Mass/Inertia $[kg][kgm^2]$.
τ	Control forces/moments [N] [Nm].
$\tau*$	Control forces/moments with adaptive term [N] [Nm].
k	Tunable gain for Sliding Mode Control.
λ	Tunable gain for Sliding Mode Control. It represents the slope of the sliding surface.
s	Sliding surface.
Φ	Tunable gain for Sliding Mode Control.
v_{max}	Maximum cruising speed [m/s] [rad/s].
Δ	Function for the minimum turn, between $\pm\pi$ [rad].
ψ	Yaw angle [rad].
θ	measured angle, used in a generalized manner for roll and pitch angles [rad].

*Corresponding author: jorge-esteban.salas-gordoniz.1@ens.etsmtl.ca

1. INTRODUCTION

In recent years, there has been a notable increase in the interest for airships and indoor blimps. Their inherent ability to remain airborne due to a buoyant gas makes them particularly appealing for autonomous missions requiring prolonged periods of time; such as environmental monitoring, climate research and telecommunication applications [1–3]. Additionally, their manoeuvrability at low speeds endows them with a distinct advantage akin to underwater robots in exploration scenarios [4]. This versatility extends further, enabling their utilization as data retrieval tools similar to satellites [3] or for exploration of planetary bodies with atmospheres [5], while the energy consumption is primarily reserved for directional adjustments and for overcoming drag and other disturbances.

The incorporation of soft membrane materials allows blimps to navigate safely around humans [6, 7], showcasing their efficacy in accessing challenging environments, including subterranean spaces, provided adequate spatial clearance [8, 9]. This attribute renders them invaluable for data retrieval missions and search and rescue operations, where traditional vehicles may face constraints.

The control of a blimp, nevertheless, is acknowledged to be a difficult task. Nonlinearities and coupled degrees of freedom make their study an interesting use-case for control; problems arise when trying to achieve good robustness to disturbances, when relating hovering and cruising flights with a smooth transition and when tuning the control strategies [10, 11].

Several control strategies have been used for the control of lighter-than-air vehicles, like blimps, including model-based controllers (Sliding Mode Control - SMC -, Model Predictive Con-

trol, Generalized Predictive Control, Terminal SMC), for which it can be troublesome to estimate the dynamic parameters [12]. These models are more often simplified, linearized and decoupled [13–15] or controllers without a model are preferred (PD, PI, PID, feedback control algorithms, use of Linear Quadratic Regulators - LQR - for optimization, gain scheduling, fuzzy control, visual servo control) [16]. In several cases, a realistic simulation environment is used to complete large number of runs before the controller is improved and tuned enough to expect a safe and robust flight on the real robot [12, 17–20].

This paper presents our intuitive controller for the smooth motion of a blimp following a path between waypoints and hovering. The controller can be tuned based on the maximum desired actuation and a maximum cruising speed, while reducing the swinging motion when hovering or when flying in steady or unsteady motions. It can also maintain the blimp at different roll and pitch angles following the mass distribution of the payload. For the altitude control, an additional simple moving average (SMA) term is included to reduce the steady-state errors to achieve the desired altitude even with fast changes in the payload.

This document is divided as follows: first, a presentation of a literature review with some of the works that helped motivate the development of our control strategies, as well as a slight discussion about the perceived difficulties and problems derived from these previous works; second, a basic presentation of the blimp robot; third, a quick presentation of the control strategies for the different requirements, followed with the experimental results and conclusions.

2. PREVIOUS WORKS

The dynamic model of an airship has been covered extensively in the literature [21], presenting similarities with the dynamic model of ocean vehicles [4]. Such models require an estimation of the dynamic parameters of the blimp, for which several works were reviewed by Li, Sharf and Nahon [22]. For the virtual or added mass/inertia (which can be roughly understood as the mass of fluid that needs to be displaced to achieve the acceleration of the robot), experimental data are preferred since fluid dynamic analysis hardly encompasses all the fluid interaction with the soft membrane and mesh structure. It can also be estimated through extrapolation from previous experiments, even if obtained from water vehicles [4, 23]. A comprehensive methodology for parameters estimation was shared for the research on the Georgia Tech Miniature Autonomous Blimp (GT-MAB), which is also intended to fly in near-human spaces. They conducted parameters identification through swinging motions [24]; an approach similar to the one we followed in our previous work [25]; and as for translational motion, GT-MAB team did parameters identification by varying the weight in a free-fall setup [26]. This last approach is, however, hardly replicable for a blimp almost three times larger than the GT-MAB. Both of these experiments by Tao et al. are extended in [27], where most of the controller tuning process was made based on the linearized transfer functions of the dynamics obtained with MatLab for each of their defined motion primitives.

With blimps, the center of mass/weight naturally tries to remain below the center of buoyancy, which can generate an oscillatory phenomenon that needs to be reduced to achieve a smooth flight. A possibility is to use a PD control to stabilize a blimp while hovering [28], which can later be stabilized to a desired angle while cruising (at constant speed) by using a PD control with moment compensation [29]. Pr. Lanteigne's group achieve this control for the pitch using a sliding ballast [30–32], which was used to improve the manoeuvrability of their robot. They tuned their PID with MatLab/Simulink and a linearized model, but then still required to be manually fine-tuned by trial and error in real experiments.

The efficacy of controllers like the PID controller, Computed Torque controller (CTC), or SMC hinges on meticulous tuning, often through trial and error [2]. While various recommendations exist for tuning these controllers, including auto-tuning techniques [4, 33–36], to the best of our knowledge no reliable method exists to effectively tune a blimp (or robot) controller in the absence of a precise dynamic model and the need for simple tuning methods is still pervasive [34]. Moreover, there is a need for approaches that can swiftly and safely achieve basic manoeuvers while maintaining general applicability in real operations.

This paper introduces straightforward insights enabling the tuning of an SMC-based controller. By modelling the controller gains with physical significance, our blimp successfully navigated between waypoints and executed path-tracking manoeuvres. Additionally, we employed intuitive mechanical strategies to mitigate swinging oscillations and to reduce steady-state errors in altitude. These innovations collectively streamline the tuning process for real-world deployments, minimizing the effort required to achieve good flight performance.

3. THE ROBOT

The robot in Fig. 1 is designed by our team for indoor usage and it is used to test the control strategies presented in this paper. It is composed of an inflatable elliptical membrane made out of polyurethane with approximated dimensions of 2 meters long, 1.5 meters wide and 0.8 meters tall, with a total mass of 1.09 kg; and a detachable gondola that contains all the hardware, with a mass of 930 grams.

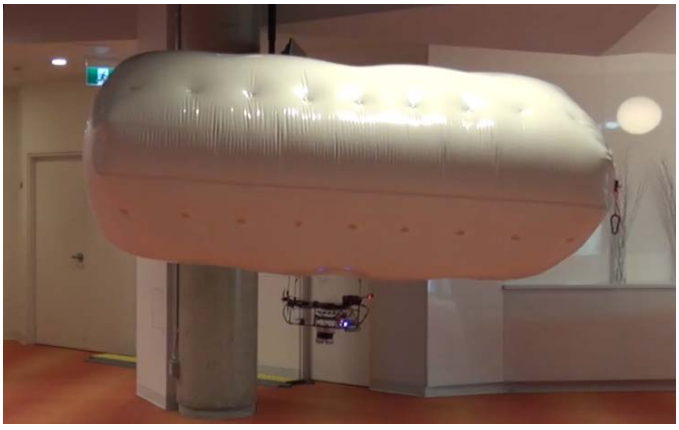

FIGURE 1: Our blimp design; a pillow-shaped polyurethane bladder with internal strings to maintain its shape and a suspended gondola with all its mechatronics underneath.

The structure of the gondola, presented in Fig. 2 is made of carbon fiber rods and 3D printed joints. For localization,

we use an Ouster OS0[1] combined with an IMU feeding our simultaneous localization and mapping stack leveraging NorLab's ICP mapper[2]. The control of the motors is achieved through a Crazyflie Bolt[3], the measurement of the attitude is made with the IMU, a VectorNav's VN-100[4], while the altitude was measured with a TFmini-S12m LiDAR ranging module[5]. Two different Lithium-ion batteries of 3500 mAh and 3000 mAh weighting less than 210 grams were used to provide the required energy. All the devices were connected via USB to a Jetson Xavier NX board[6] integrating Wi-Fi and Bluetooth capabilities to communicate with a groundstation computer in charge of controlling the robot. All the SLAM and control is achieved within ROS[7].

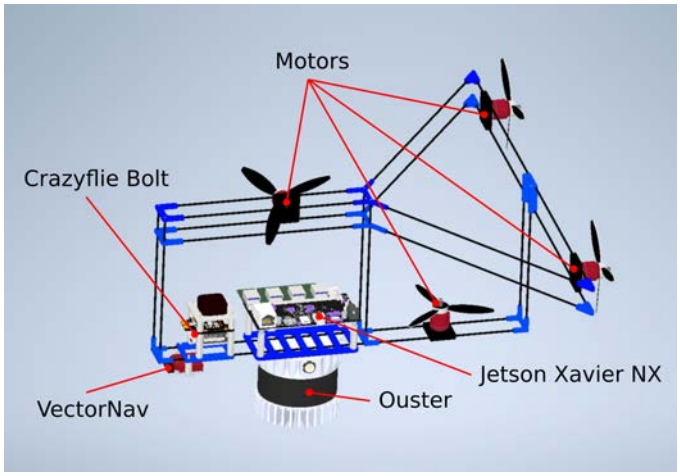

FIGURE 2: Simplified CAD design of the gondola with its parts. Cables and batteries are omitted.

4. CONTROL

4.1 Rethinking Sliding Mode Control

SMC is a well recognized robust model-based control strategy in which the system is forced towards a sliding surface where $s = 0$ and it is defined as $s = \lambda\tilde{x} + \dot{\tilde{x}}$, where the error $\tilde{x}$ is defined as $\tilde{x} = x - x_d$ (for the state x, being the subscript d for 'desired') [4, 33] . Then, for a dynamic system:

$$m\ddot{x} = F(\vec{x}, t) + \tau(\vec{x}) \tag{1}$$

with m being the mass/inertia, F the forces/moments on the system (not related to control), $\vec{x}$ the state vector of the system and $\tau(\vec{x})$ is the control forces/moments, given by:

$$\tau(\vec{x}) = \hat{m}(\ddot{x}_d - \lambda\dot{\tilde{x}} - k \cdot sign(s)) - \hat{F}(\vec{x}, t) \tag{2}$$

where

$$sign(s) = \begin{cases} 1, & \text{if } s > 0 \\ 0, & \text{if } s = 0 \\ -1, & \text{if } s < 0 \end{cases} \tag{3}$$

[1]https://ouster.com/products/hardware/os0-lidar-sensor
[2]https://github.com/norlab-ulaval/norlab_icp_mapper
[3]https://www.bitcraze.io/products/crazyflie-bolt-1-1/
[4]https://www.vectornav.com/products/detail/vn-100
[5]https://en.benewake.com/TFminiS/index.aspx?proid=325
[6]https://www.nvidia.com/en-us/autonomous-machines/embedded-systems/jetson-xavier-series/
[7]https://www.ros.org

while $\hat{m}$ and $\hat{F}(\vec{x}, t)$ are the estimations of m and $F(\vec{x}, t)$, respectively.

This controller type has been successfully applied for underwater and airship robots [16, 33], but it has a major drawback: it generates fast and strong oscillations in the control forces/moments near the sliding surface, referred to as 'chattering'. A potential fix to this issue is to replace the *sign* function with a saturation function such as:

$$sign(s) \rightarrow sat(s/\Phi) \tag{4}$$

where:

$$sat(s/\Phi) = \begin{cases} 1, & \text{if } s/\Phi > 1 \\ s/\Phi, & \text{if } -1 \leq s/\Phi \leq 1 \\ -1, & \text{if } s/\Phi < -1 \end{cases} \tag{5}$$

having Φ as a tunable gain related to the width of a region around $s = 0$ in the phase plane.

Using the saturation function, we focus on the case where the desired state is at rest ($\ddot{x}_d, \dot{x}_d = 0$); writing the control equation as:

$$\tau(\vec{x}) = \hat{m}(-\lambda\dot{x} - k \cdot sat(s/\Phi)) - \hat{F}(\vec{x}, t) \tag{6}$$

Finally, if we assume the system is perfectly compensated ($\hat{F}(\vec{x}, t) = F(\vec{x}, t)$), then the dynamic equation becomes:

$$m\ddot{x} = \hat{m}(-\lambda\dot{x} - k \cdot sat(s/\Phi)) \tag{7}$$

For $|s/\Phi| > 1$, Eq. (7) is similar to the equation of free-falling motion with a linear dampening term, since the saturation term becomes equal to ± 1. Therefore, we can rewrite $\lambda = k/v_{max}$, where $v_{max} > 0$ represents the magnitude of the maximum cruising speed. This also highlights $\hat{m}k$ as the maximum desired force/moment. From this, we can secure the robustness of the system when $|s/\Phi| > 1$ for $k\hat{m} > |F(\vec{x}, t) - \hat{F}(\vec{x}, t)|$; and if the system is not perfectly compensated, we expect that the robot will reach slower cruising speeds than $\pm v_{max}$.

Note that, when the system achieves constant speed, the control forces have a magnitude equal to $F(\vec{x}, t)$, which results in the control actuation compensating the external forces (like drag) while in cruising motion, minimizing additional energy requirements; and once $|s/\Phi| < 1$, the control system becomes a PD controller.

This easy method allows us to hover and to travel at slow speeds with minimum tuning effort, contrasting with advanced SMC strategies that more often try to achieve faster convergences by including additional terms and tunable gains [35, 37].

4.2 Ideal Stop

Considering a perfectly compensated system, as in Eq. (7), and assuming $m = \hat{m}$, it is then useful to investigate the condition in which the system stops at a desired position once entered in the region where $s/\Phi < 1$ at a velocity $\pm v_0$. When solving the controlled system, the solution is:

$$\tilde{x} = \pm\frac{\Phi^2 e^{-\frac{kt}{\Phi}}}{k - \lambda\Phi} \pm \frac{(-\Phi k - k v_0 + \Phi\lambda v_0)e^{-\lambda t}}{(k - \lambda\Phi)\lambda} \tag{8}$$

and the system will reach the sliding surface following:

$$s = \mp\Phi e^{-\frac{kt}{\Phi}} \tag{9}$$

This underscores the significance of leveraging the saturation region, particularly in achieving exponential convergence to the desired position with zero velocity, irrespective of the choice of Φ (provided $m = \hat{m}$). For slower motions, a higher Φ and lower k prove advantageous (contrary to the requirements for faster convergence). However, opting for a smaller k compromises the system's robustness.

Consequently, the system's ability to maintain gradual cruising speeds and halt precisely at designated positions enables safe closed-loop experiments across various velocities. This approach facilitates the study of both drag behavior and the system's added mass, paving the way for updating the control system to incorporate drag compensation with experimental data. Such adaptability ensures the system's responsiveness to unstructured environmental conditions and secures its overall performance.

4.3 Adaptive term for the weight

While the motion in X, Y and Z axes can be achieved with the control presented in Eq. (7), by replacing x with y and z, the system will lose robustness to maintain the desired altitude as the helium leaks or when changing the payload in the air, even more in the region $|s/\Phi| < 1$ where the robustness of SMC is not secured. To solve this problem, our first methods included weighting the blimp before each flight and statically balancing it in the air (pitch and roll angles); this affects the weight and, due to the permeability of the membrane, this quickly becomes a tedious task for several days of experiments that also require subsequent updates in the tuning.

While this altitude correction could be achieved through an integral term (as in a PID control), properly tuning the controller is an arduous task that delays the test of the prototype. Therefore, we considered a more intuitive method to simplify this process, as presented in Fig. 3.

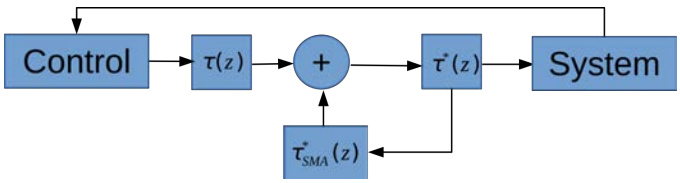

FIGURE 3: General control diagram to compensate the weight of the blimp.

The previous figure shows that, after calculating the control forces $\tau(z)$ we add the simple moving average (SMA) of the calculated $\tau^*(z)$ before applying it to the system, equal to $\overline{\tau}^*_{SMA}(z)$. The origin of this method comes from the idea that a PD controller might stabilize the robot at an altitude at which the control forces are equal to the net weight (weight minus buoyancy); therefore, the force we need to compensate the net weight is equal to the applied force at this stabilized altitude. Since the stabilization might not be perfect and present a degree of oscillations (in terms of motion and actuation forces), an average is used to filter the applied force before being reintroduced in the control. Finally, using a simple average has two main problems: it can result in having a massive list of applied forces (requiring more control memory) and; the longer the list, the system becomes less sensitive to future changes. These problems can be reduced with a SMA instead of a simple average, where we can select the length of the list and hence, the strength of the applied filter. The results of both the averaging and SMA term is being displayed in Section 5.2.

4.4 Generalized Roll and Pitch Stabilization

It is well known that the motion of a blimp is coupled: the position of the center of weight below the center of buoyancy added to the position of the motors in a gondola are so that any translation manoeuvre also impacts the attitude of the system, resulting in oscillations or swinging motions that need to be mitigated to achieve a smooth movement of the robot. The current state-of-the-art stabilization methods for roll and pitch of a blimp consider only the steady states [28, 29] and require a good estimation of the drag, the mass and inertia parameters: geometrical center, center of mass, position of the applied propulsion, as well as weight and buoyancy. Since the drag depends on the velocity, an extended study (or test/simulation campaign) is required for each target velocity.

Instead, we propose a simple method that can be generalized outside the steady-state motion and does not rely on accurate knowledge of the drag effect nor arbitrarily enforces a desired pitch and roll angles. For this, we have the following considerations:

1) When we make a system fly from the ground, unless it has been perfectly balanced, the system will tend towards different roll and pitch angles than the ones it had while in contact with the ground; stabilizing at these ground angles will force undesirable moments in the air.

2) We assume that, when in motion, the system will naturally tend to new sets of stable angles that are affected by the drag, control forces, weight, buoyancy and the geometry of the system; and then, even if the system starts oscillating, the oscillations will be produced around these stable angles.

Then, we can offer a first stabilization control for the angles as a PD control with SMA terms (which automatically updates the desired angles and rates based on the average of a user defined sliding time window of the previous measurements):

$$\tau_\theta = P\left(\theta_{SMA} - \theta\right) + D\left(\dot{\theta}_{SMA} - \dot{\theta}\right) \tag{10}$$

where θ_{SMA} and $\dot{\theta}_{SMA}$ represent the SMA terms of θ and $\dot{\theta}$, respectively (without lost of generality for roll and pitch angles), with P and D being the proportional and differential gains, respectively. This means that the controller will try to make the system achieve the angle with respect to a low pass-filter of the measurements obtained through the SMA terms, proposition that can be used while flying in steady states or while accelerating. This provides a system that tries to maintain the averaged angles and averaged rotational ratios. The idea behind the control equation in Eq. (11) comes from the naturally produced damped oscillation due to drag effects: if we assume a damped sinusoidal oscillation and obtain its average in the entire motion, this average will tend towards the center of oscillation and the time it will take to reach it will depend on how large are the older angles in relation with the newest ones; in this case, the time can be reduced by neglecting some of the oldest values in favor of the newest ones,

which we can do by using SMA. A similar behaviour occurs with the SMA of the angular rates: in steady state, it is expected that the amplitude of the angular velocities will decay and with it, its average will also tend to zero; in accelerated motion, the amplitude of angular rate can increase and decrease, so we would like that the system follows the general motion, which we obtain again through the SMA of the angular rates.

In fact, the proportional term in Eq. (10) is not mandatory since the system will be naturally forced due to gravity, drag, buoyancy, the difference between the center of buoyancy and center of gravity, and the position of the propellers. Therefore, we can use only the differential term, which will help dissipating kinematic energy from the system when achieving steady motions, or it will force the system to maintain an average of the previous angular velocities.

An additional practical problem appears when the oscillations are small and of higher frequencies than the control frequencies of the actuators and the differential gain is too high: at the end of the oscillation, the control system might continue pushing the system towards the center of oscillation with the possibility of destabilizing the pitch and roll and forcing the system to enter cycles of low and high amplitudes. In the case of larger oscillations, this could be ignored since longer arches will still allow to compensate for this effect, but this is not possible for smaller angles. To cope with this, we propose the following control equation:

$$\tau_\theta = D\left(\dot{\theta}_{SMA} - \dot{\theta}\right) \cdot |sin\left(\theta_{SMA} - \theta\right)| \tag{11}$$

This previous equation was used to allow high values of D and to quickly dampen the oscillations when the system is away from the equilibrium while flying with bounded pitch and roll angles, between $\pm\pi/2$ (in all of our experiments, the pitch and roll angles never go over 0.7 radians). Additionally, the inclusion of the *sin* term is used to reduce the action of the differential term when close to the stable orientation, to reduce the possibility of exciting the oscillation. In exchange, small amplitude oscillations are less damped than larger ones.

5. EXPERIMENTS

The following sub-sections showcase the use of our controllers in real deployment tests alongside our observations.

5.1 Planar

From Eq. (6), we select the version without model, $\hat{m} = 1$, nor estimations for XYZ axes and for the yaw (ψ), presenting the equation for the X-axis (without loss of generality for the other axes - more about the Z-axis in Section 5.2):

$$\tau(x) = -\frac{k}{v_{max}}\dot{x} - k \cdot sat(s/\Phi) \tag{12}$$

To tune this controller, our methodology is simple: if the overshoot is too high, there are two options: to increase the value of k (which was actually set to the capacity of the motors), or to reduce the value of v_{max}. Finally, the gain selection was $k = 0.7$ N and $v_{max} = 0.5$ m/s for X and Y axes, while $k = 0.5$ N for the altitude, with the same speed; and for the yaw, $k = 0.266$ Nm, which came from the maximum applicable force multiplied by the distance between the motors and $v_{max} = 1.57$ rad/s. The value of Φ was arbitrarily selected as 1 for all of them, while these tuning conditions remained constant for all the experiments presented in this document.

5.1.1 Square. At one meter high, the system is tasked to do a square of 3 meters side. Once the blimp enters the region $|s/Phi| < 1$ for X and Y axes, it will wait 30 seconds to stabilize itself (hovering) and then it will proceed to the next point. This motion is produced without changes in the yaw.

The results show that the overshoot did not go over 15 cm for the X-axis and 25 cm for the Y-axis, as presented in Fig. 4. While the motion was defined for a maximum velocity of 0.5 m/s, the phase diagram in Fig. 5 shows that the velocity was closer to 0.4 m/s, which we can attribute to drag effects, since they were not compensated.

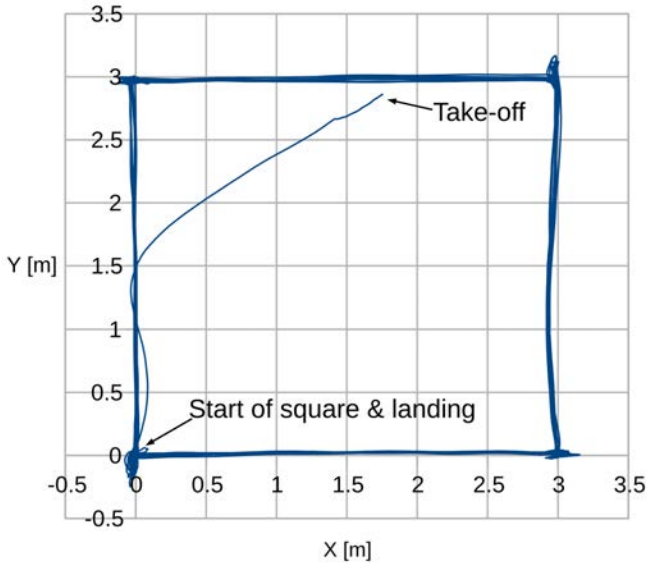

FIGURE 4: Square motion. The system started from the ground, flew up to 1 meter height and proceeded to complete 10 full squares. The total time of the manoeuvre was 25 minutes (from takeoff to landing).

Then, we can observe the relation between the applied force and the value of s in Fig. 6. If we start from $s = \pm 4$ and follow the curve towards $s = \pm 1$, we can observe that the force converges towards a constant which, combined with the constant velocity achieved in Fig. 5, allows us to conclude that the terminal velocity was achieved. On another hand, the achieved force was still bigger than $\hat{m}k$ (the maximum desired force), which can result after surpassing the desired position due to the controller trying to stop the robot and push it back.

While these results are simple and fall within the expected behaviour for a single combination of k and v_{max}, we expect that extending these experiments with different gains will allow us to estimate the drag behaviour of our blimp while maintaining the closed-loop position control, which can help guaranteeing the safety of the experiments.

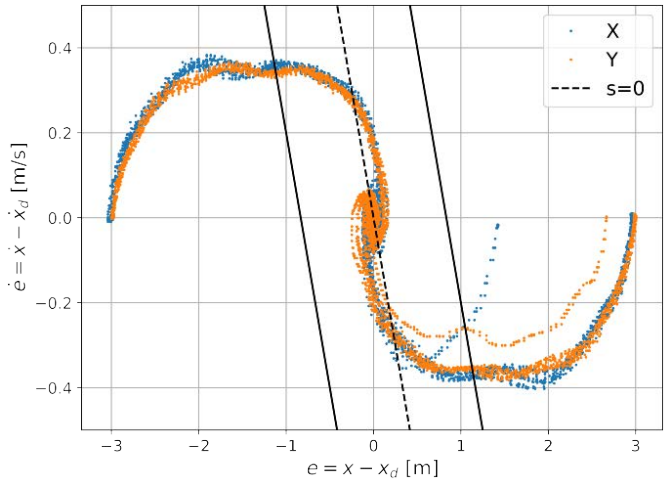

FIGURE 5: Phase diagram for the square motion with length of 3 m. In blue for the *X*-axis and in orange for the *Y*-axis. The central dashed line represents $s = 0$ and the black diagonal lines represents the values of $\Phi = \pm 1$.

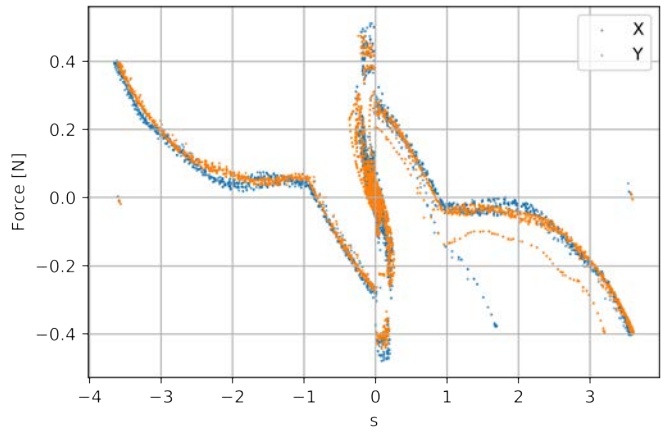

FIGURE 6: Force versus *s*. In blue for the *X*-axis and in orange for the *Y*-axis.

5.1.2 Circle. At one meter high, the system is tasked to do a circle of 4 meters diameter. To do this, the circle was divided in 200 waypoints and once the system gets to 10 cm from its current desired waypoint, it then switches to the next.

While flying in circle, the yaw changed to maintain the blimp aligned with its trajectory, using the following formula:

$$\Delta(\psi) = 2atan\left(tan\left(\frac{\psi_d - \psi}{2}\right)\right) \tag{13}$$

to calculate the minimum rotation between $\pm\pi$.

The result of the path is presented in Fig. 7, where we observe that the trajectory radius remained mostly between 1.97 and 2 meters and the path was consistently followed for 10 full circles in the air.

While the blimp was able to maintain a constant motion, the arbitrary selection of $\Phi = 1$ seemed inadequate for the yaw control, since the system remained in the region $|s/\Phi| < 1$ where it behaved as a PD control, which meant a lateral range from

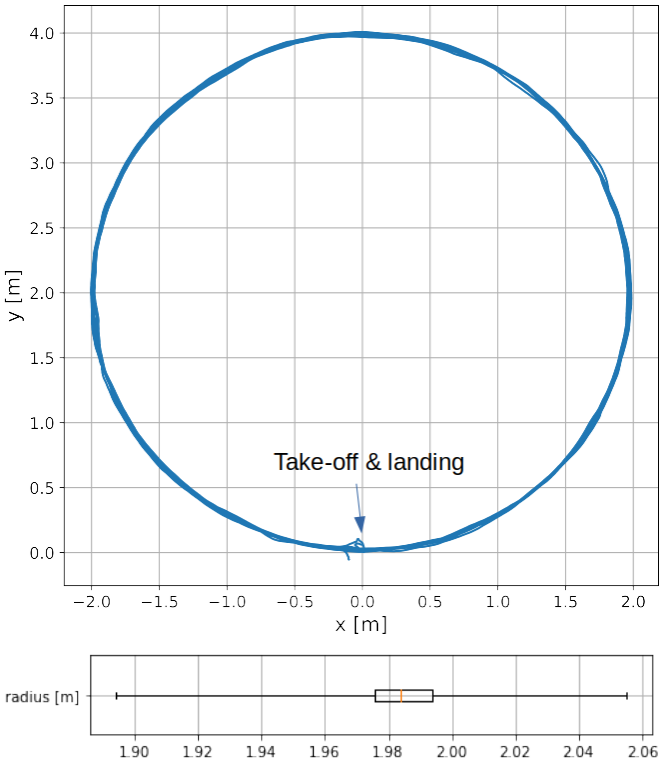

FIGURE 7: Circle. The system started from the ground, flew up to 1 meter high and proceeded to do 10 full circles. The total time of the manoeuvre was of 26 minutes (from take-off to landing).

the sliding curve of about 5.9 radians (about 338 degrees). This produced an average $\Delta(\psi)$ of 0.34 radians (about 19.5 degrees), with a standard deviation of 0.126 radians (about 7.2 degrees). Nevertheless, due to the slow motion desired for the blimp, the error in the yaw did not seem noticeable during the experiments. In this case, a smaller Φ value could have improved these results, for which further studies are still needed to evaluate the adequacy of defining the region $|s/\Phi| < 1$ to reduce these differences in path following motions, as well as to identify the behaviour of the control forces/moments when working with and without a model.

Finally, in long duration tests for the circular path, the blimp flew continuously up to 41 minutes with a single charge, traveling an estimated distance of 280 meters, equivalent to an average of 0.1138 m/s (about 0.41 km/h).

5.2 Altitude

Using Eq. (12) (for the Z-axis) and the control strategy shown in Fig. 3, we experimented by using the averaging in the entire motion while comparing the same control without this term. Figure 8 shows that it is possible to reduce the steady-state error due to the weight but the overshoot is excessive for our requirements when it is applied from the ground and for the entire duration of the motion.

Therefore, we used an SMA term (instead of the averaging) after 40 seconds, time at which it was considered enough to stabilize the blimp at any resultant altitude, while considering a list of the last 400 terms (the measurements of the last 10 seconds with a control frequency of 40 Hz). As well, to avoid a quick and

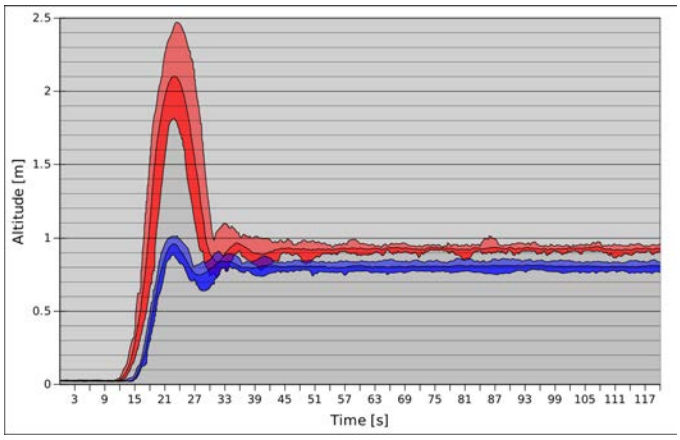

FIGURE 8: Averaging in the entire motion. Blue without averaging. Red with averaging. Limits represent the maximum, minimum and average of 10 experiments. Trying to fly up to 1 m.

strong correction, this list was first initialized with 400 zeroes and each new measurement replaced the oldest values of the list, until the force was finally equal to the net weight (weight minus buoyancy). The results proved to always achieve and maintain our desired height. We tested this strategy while removing and adding weights of 25 grams to evaluate its robustness, while also evaluating the capability of our system to maintain any arbitrary pitch and roll angles due to these changes (more in Section 5.3.2). The results for the altitude experiments presented in Fig. 9 proved that the strategy was effective to approximate the system to the desired altitude of 1 meter, even with changes in the weight. Nevertheless, it is important to note that if the total net weight to lift surpasses the value of $\hat{m}k$, the system will precipitate.

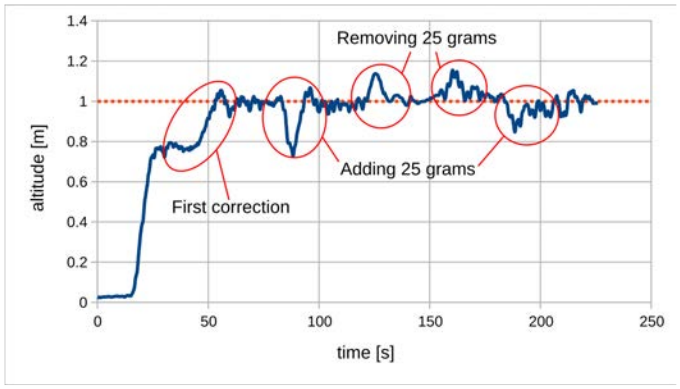

FIGURE 9: Stabilization (focus on altitude). The system must achieve and remain at an altitude of 1 meter even with sudden changes in the weight.

5.3 Swinging Stabilization

Using the control for roll and pitch stabilization as presented in Eq. (11), with angle measurements done at 400 Hz, the selected SMA term considered a list of 40 measurements for the roll and pitch angles (0.1 seconds) and 500 measurements for the angular rates (1.25 seconds). The differential gains were 70.0 for the roll and 50.0 for the pitch, which were maintained for the entirety of the experiments presented in this document.

5.3.1 Hovering. The effect of this stabilization method can be contrasted with the natural damping, as provided in Fig. 10, where the system was manually forced to oscillate once in the air. A video with an example of the stabilization after a forced disturbance is presented in [38]. While the results show that it is indeed possible to reduce the oscillations, the roll presented a smaller dampening effect than the pitch, even with a higher selected gain, which we could associate with the fact that there is a single motor shared for roll and Y-axis motion and it can saturate easier than for the X-axis motion, where two motors are used.

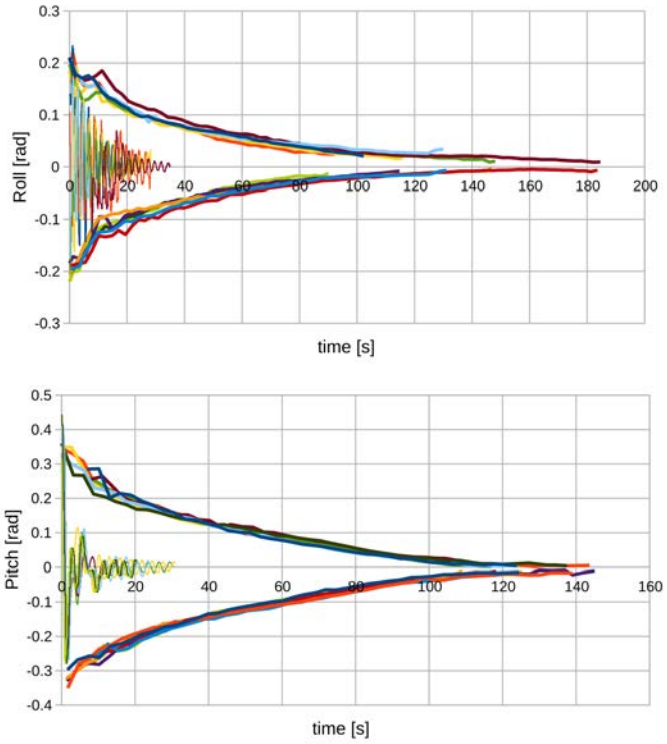

FIGURE 10: Pitch and Roll stabilization. Outside curves, free oscillation decay; inside curves, stabilized oscillations. The start of the stabilized oscillations is approximately equal to the magnitude of the free oscillations. The experiments were stopped when the oscillations were visually negligible, resulting in shorter durations for the controlled stabilization experiments.

5.3.2 Stabilization with Weight Changes. As an extension of the experiment for altitude correction presented in Fig. 9, stabilization was needed to secure that the system will remain at every new orientation without large oscillations and without resisting after the weights are added or removed.

This test, presented in Fig. 11, was sequentially completed by letting the system go to the air, adding 25 grams in the front-right (positive change of pitch and roll), removing 25 grams from the back-left (positive change of pitch and roll), removing 25 grams from the front right (negative change for pitch and roll) and finally adding 25 grams in the back-left (negative change for pitch and roll). The results show that the starting amplitude of the

oscillations due to the change of weight where smaller than 0.04 radians (2.29 degrees) and it was still reduced to less than 0.01 radians (about 0.57 degrees), both values determined about the SMA term identified as 'desired' in Fig. 11, which is considered as satisfactory for our stabilizing control. Therefore, using the control equation presented in Eq. (11) we could effectively reduce the oscillation for any new orientation achieved by the blimp in pitch and roll due to changes in the weight of the system at different positions on the robot by only applying a single differential term, while it is still compatible with the altitude stabilization strategy as shown in the previous Fig. 9.

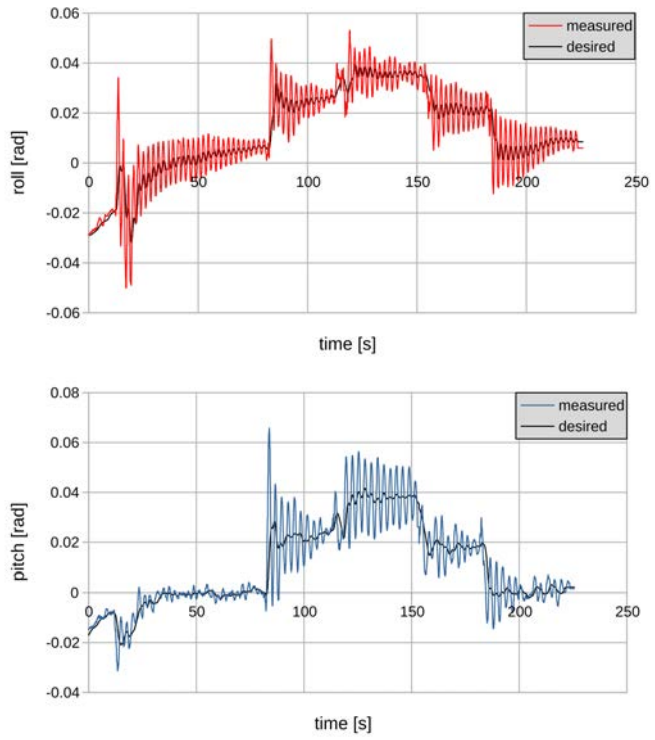

FIGURE 11: Altitude correction, focus on roll and pitch stabilization with weights changes. The central line is obtained from the applied filter of the measurements.

6. CONCLUSION

Based on Sliding Mode Control with saturation reaching law, we presented a controller that does not rely on a robot's accurate dynamic model and is still capable of achieving good flight performance for an indoor blimp. Two flight modes were tested: path tracking between waypoints and hovering.

We considered the flight scenario of position reaching with no final velocity which allowed us to rewrite the control gains based on the maximum desired forces and the maximum cruising speed, which in turns minimize the tuning efforts. The gains obtained were applicable to two different paths, a square and a circle in the air.

For altitude control, we added an adaptive simple moving average term to the previous control strategy based on the averaging of the previously applied forces, which allows to intuitively correct the effects of the weight and to reduce the steady-state errors. We showed from experiments that it works even when changing the weight of the system in the middle of the flight and avoids the need to tune an integral term.

To reduce undesirable swinging motion, a single nonlinear dampening term was applied to the pitch and roll angles control, which considers the desired pitch and roll angular velocities obtained through a simple moving average; a behavior similar to a low-pass filter of the measurements. This allows to reduce large oscillations while hovering, as well as for steady and unsteady motions, as it maintains natural pitch and roll angles without forcing an arbitrary attitude.

Moving forward, this controller will serve as a pivotal tool for the estimation of the parameters of the dynamic model, enabling the refinement of our control strategy towards a more robust, model-based approach. Additionally, we will explore its potential in achieving precise velocity control at specified positions, providing valuable insights into optimizing the selection of the gain Φ for the saturation term. Moreover, we aim to leverage this methodology as a rapid testing tool for our forthcoming prototypes, streamlining the iterative design process and facilitating quicker validation of our innovations. By integrating this controller into our development pipeline, we anticipate significant advancements in both control strategy sophistication and prototype iteration efficiency.

REFERENCES

[1] Elfes, A., Siqueira Bueno, S., Bergerman, M. and Ramos, J.G. "A semi-autonomous robotic airship for environmental monitoring missions." *Proceedings. 1998 IEEE International Conference on Robotics and Automation (Cat. No.98CH36146)*, Vol. 4: p. 3449–3455. 1998. IEEE, Leuven, Belgium. DOI 10.1109/ROBOT.1998.680971. URL http://ieeexplore.ieee.org/document/680971/.

[2] De Paiva, E.C., Bueno, S.S., Gomes, S.B.V., Ramos, J.J.G. and Bergerman, M. "A control system development environment for AURORA's semi-autonomous robotic airship." *Proceedings 1999 IEEE International Conference on Robotics and Automation (Cat. No.99CH36288C)*, Vol. 3: p. 2328–2335. 1999. IEEE, Detroit, MI, USA. DOI 10.1109/ROBOT.1999.770453. URL http://ieeexplore.ieee.org/document/770453/.

[3] Bueno, Samuel S, Azinheira, Jose R, Ramos, Josue Jr G, de Paiva, Ely C, Rives, Patrick, Elfes, Alberto, Carvalho, Jose R H and Silveira, Geraldo F. "Project AURORA: Towards an Autonomous Robotic Airship." (2002).

[4] Fossen, Thor I. *Handbook of Marine Craft Hydrodynamics and Motion Control*, 1st ed. Wiley (2011). DOI 10.1002/9781119994138. URL https://onlinelibrary.wiley.com/doi/book/10.1002/9781119994138.

[5] Elfes, Alberto, Bueno, Samuel S., Bergerman, Marcel, De Paiva, Ely C., Ramos, Josué G., Jr. and Azinheira, José R. "Robotic Airships for Exploration of Planetary Bodies with an Atmosphere: Autonomy Challenges." *Autonomous Robots* Vol. 14 No. 2/3 (2003): p. 147–164. DOI 10.1023/A:1022227602153.

[6] Burri, M., Gasser, L., Kach, M., Krebs, M., Laube, S., Ledergerber, A., Meier, D., Michaud, R., Mosimann, L., Muri,

L., Ruch, C., Schaffner, A., Vuilliomenet, N., Weichart, J., Rudin, K., Leutenegger, S., Alonso-Mora, J., Siegwart, R. and Beardsley, P. "Design and control of a spherical omnidirectional blimp." *2013 IEEE/RSJ International Conference on Intelligent Robots and Systems*: p. 1873–1879. 2013. IEEE, Tokyo. DOI 10.1109/IROS.2013.6696604. URL http://ieeexplore.ieee.org/document/6696604/.

[7] St-Onge, David, Brèches, Pierre-Yves, Sharf, Inna, Reeves, Nicolas, Rekleitis, Ioannis, Abouzakhm, Patrick, Girdhar, Yogesh, Harmat, Adam, Dudek, Gregory and Giguère, Philippe. "Control, localization and human interaction with an autonomous lighter-than-air performer." *Robotics and Autonomous Systems* Vol. 88 (2017): p. 165–186. DOI 10.1016/j.robot.2016.10.013.

[8] Huang, Yi-Wei, Lu, Chen-Lung, Chen, Kuan-Lin, Ser, Po-Sheng, Huang, Jui-Te, Shen, Yu-Chia, Chen, Pin-Wei, Chang, Po-Kai, Lee, Sheng-Cheng and Wang, Hsueh-Cheng. "Duckiefloat: a Collision-Tolerant Resource-Constrained Blimp for Long-Term Autonomy in Subterranean Environments." No. arXiv:1910.14275 (2019). URL http://arxiv.org/abs/1910.14275. ArXiv:1910.14275 [cs].

[9] Wang, Hsueh-Cheng. "A Heterogeneous Unmanned Ground Vehicle and Blimp Robot Team for Search and Rescue using Data-driven Autonomy and Communication-aware Navigation." *Field Robotics* (2022).

[10] De Paiva, Ely Carneiro, Benjovengo, Fábio and Bueno, Samuel Siqueira. "SLIDING MODE CONTROL FOR THE PATH FOLLOWING OF AN UNMANNED AIRSHIP." *IFAC Proceedings Volumes* Vol. 40 No. 15 (2007): p. 221–226. DOI 10.3182/20070903-3-FR-2921.00040.

[11] Paiva, Ely, Benjovengo, Fabio, Bueno, Samuel and Ferreira, Paulo. "Sliding Mode Control Approaches for an Autonomous Unmanned Airship." *18th AIAA Lighter-Than-Air Systems Technology Conference*. 2009. American Institute of Aeronautics and Astronautics, Seattle, Washington. DOI 10.2514/6.2009-2869. URL https://arc.aiaa.org/doi/10.2514/6.2009-2869.

[12] Liu, Yu Tang, Price, Eric, Black, Michael J. and Ahmad, Aamir. "Deep Residual Reinforcement Learning based Autonomous Blimp Control." *2022 IEEE/RSJ International Conference on Intelligent Robots and Systems (IROS)*: p. 12566–12573. 2022. IEEE, Kyoto, Japan. DOI 10.1109/IROS47612.2022.9981182. URL https://ieeexplore.ieee.org/document/9981182/.

[13] Sami, Abdul, Reddy, N Alekhya, Reddy, K Akhil, Bhushan, Kanaka, Mudhiraj, Rakesh, Prudhvi, Bheemarasetty, Kumar, Pikkalkar Praveen, Sai, G, Kumar, Pavan and Teja, Katte Abhilash. "A Brief Study on Airship Using Aerospace, Electronic and Communication Applications." Vol. 5 No. 4 (2015).

[14] Zuo, Zongyu, Song, Jiawei, Zheng, Zewei and Han, Qing-Long. "A survey on modelling, control and challenges of stratospheric airships." *Control Engineering Practice* Vol. 119 (2022): p. 104979. DOI 10.1016/j.conengprac.2021.104979.

[15] Atyya, Mohamed, ElBayoumi, Gamal M. and Lotfy, Mohamed. "Optimal tracking control for underactuated airship." *Journal of Engineering and Applied Science* Vol. 71 No. 1 (2024): p. 2. DOI 10.1186/s44147-023-00324-3.

[16] Herman, Przemyslaw. *Various Control Strategies*. Springer Tracts in Mechanical Engineering, Springer Tracts in Mechanical Engineering. Springer International Publishing, Cham (2022): p. 75–109. DOI 10.1007/978-3-030-94647-0_5. URL https://link.springer.com/10.1007/978-3-030-94647-0_5.

[17] Zufferey, Jean-Christophe, Guanella, Alexis, Beyeler, Antoine and Floreano, Dario. "Flying over the reality gap: From simulated to real indoor airships." *Autonomous Robots* Vol. 21 No. 3 (2006): p. 243–254. DOI 10.1007/s10514-006-9718-8.

[18] Seguin, Landan, Zheng, Justin, Li, Alberto, Tao, Qiuyang and Zhang, Fumin. "A Deep Learning Approach to Localization for Navigation on a Miniature Autonomous Blimp." *2020 IEEE 16th International Conference on Control Automation (ICCA)*: p. 1130–1136. 2020. IEEE, Singapore. DOI 10.1109/ICCA51439.2020.9264514. URL https://ieeexplore.ieee.org/document/9264514/.

[19] Bellemare, Marc G., Candido, Salvatore, Castro, Pablo Samuel, Gong, Jun, Machado, Marlos C., Moitra, Subhodeep, Ponda, Sameera S. and Wang, Ziyu. "Autonomous navigation of stratospheric balloons using reinforcement learning." *Nature* Vol. 588 No. 7836 (2020): p. 77–82. DOI 10.1038/s41586-020-2939-8.

[20] Liu, Yu Tang, Price, Eric, Goldschmid, Pascal, Black, Michael J. and Ahmad, Aamir. "Autonomous Blimp Control using Deep Reinforcement Learning." No. arXiv:2109.10719 (2021). URL http://arxiv.org/abs/2109.10719. ArXiv:2109.10719 [cs, eess].

[21] Bestaoui Sebbane, Yasmina, Tzafestas, S. G., Antsaklis, P., Borne, P., Caldwell, D. G., Chen, C. S., Fukuda, T., Monaco, S., Schmidt, G., Harashima, F., Sinha, N. K., Tabak, D. and Valavanis, K. *Lighter than Air Robots*. Vol. 58 of *Intelligent Systems, Control and Automation: Science and Engineering*. Springer Netherlands, Dordrecht (2012). DOI 10.1007/978-94-007-2663-5. URL http://link.springer.com/10.1007/978-94-007-2663-5.

[22] Li, Yuwen, Nahon, Meyer and Sharf, Inna. "Airship dynamics modeling: A literature review." *Progress in Aerospace Sciences* Vol. 47 No. 3 (2011): p. 217–239. DOI 10.1016/j.paerosci.2010.10.001.

[23] Korotkin, A. I. *Added masses of ship structures*. Fluid mechanics and its applications, Springer, United Kingdom (2009).

[24] Tao, Qiuyang, Cha, Jaeseok, Hou, Mengxue and Zhang, Fumin. "Parameter Identification of Blimp Dynamics through Swinging Motion." *2018 15th International Conference on Control, Automation, Robotics and Vision (ICARCV)*: p. 1186–1191. 2018. IEEE, Singapore. DOI 10.1109/ICARCV.2018.8581376. URL https://ieeexplore.ieee.org/document/8581376/.

[25] Salas Gordoniz, Jorge Esteban, Reeves, Nicolas and St-Onge, David. "Scutigera: Design, Modeling, and Experiments for an Artistic Multibody Airship Concept." *Jour-*

nal of Mechanisms and Robotics Vol. 14 No. 4 (2022): p. 041004. DOI 10.1115/1.4053926.

[26] Tao, Qiuyang, Hou, Mengxue and Zhang, Fumin. "Modeling and Identification of Coupled Translational and Rotational Motion of Underactuated Indoor Miniature Autonomous Blimps." *2020 16th International Conference on Control, Automation, Robotics and Vision (ICARCV)*: p. 339–344. 2020. IEEE, Shenzhen, China. DOI 10.1109/ICARCV50220.2020.9305371. URL https://ieeexplore.ieee.org/document/9305371/.

[27] Tao, Qiuyang. "Design and Control of an Indoor Miniature Autonomous Blimp." Ph.D. Thesis, Georgia Tech University. 2020.

[28] Tao, Qiuyang, Tan, Tun Jian, Cha, Jaeseok, Yuan, Ye and Zhang, Fumin. "Modeling and Control of Swing Oscillation of Underactuated Indoor Miniature Autonomous Blimps." *Unmanned Systems* Vol. 09 No. 01 (2021): p. 73–86. DOI 10.1142/S2301385021500060.

[29] Tao, Qiuyang, Wang, Junkai, Xu, Zheyuan, Lin, Tony X., Yuan, Ye and Zhang, Fumin. "Swing-Reducing Flight Control System for an Underactuated Indoor Miniature Autonomous Blimp." *IEEE/ASME Transactions on Mechatronics* Vol. 26 No. 4 (2021): p. 1895–1904. DOI 10.1109/TMECH.2021.3073966.

[30] Alsayed, Ahmad and Lanteigne, Eric. "Experimental pitch control of an unmanned airship with sliding ballast." *2017 International Conference on Unmanned Aircraft Systems (ICUAS)*: p. 1640–1646. 2017. IEEE, Miami, FL, USA. DOI 10.1109/ICUAS.2017.7991326. URL https://ieeexplore.ieee.org/document/7991326/.

[31] Lanteigne, Eric, Alsayed, Ahmad, Robillard, Dominic and Recoskie, Steven G. "Modeling and Control of an Unmanned Airship with Sliding Ballast." *Journal of Intelligent Robotic Systems* Vol. 88 No. 2–4 (2017): p. 285–297. DOI 10.1007/s10846-017-0533-6.

[32] Lanteigne, Eric and O'Reilly, Joshua. "Multibody Dynamic Modeling and Control of an Unmanned Aerial Vehicle under Non-Holonomic Constraints." *2020 International Conference on Unmanned Aircraft Systems (ICUAS)*: p. 316–321. 2020. IEEE, Athens, Greece. DOI 10.1109/ICUAS48674.2020.9213950. URL https://ieeexplore.ieee.org/document/9213950/.

[33] Slotine, J.-J. E. and Li, Weiping. *Applied nonlinear control*. Prentice Hall, Englewood Cliffs, N.J (1991).

[34] Åström, Karl J., Hägglund, Tore and Åström, Karl J. *PID controllers*, 2nd ed. International Society for Measurement and Control, Research Triangle Park, N.C (1995).

[35] Fallaha, Charles J., Saad, Maarouf, Kanaan, Hadi Youssef and Al-Haddad, Kamal. "Sliding-Mode Robot Control With Exponential Reaching Law." *IEEE Transactions on Industrial Electronics* Vol. 58 No. 2 (2011): p. 600–610. DOI 10.1109/TIE.2010.2045995.

[36] Xuan-Mung, Nguyen, Nguyen, Ngoc Phi, Pham, Dinh Ba, Dao, Nhu Ngoc, Ngoc, Thanh Ha Le Nhu, Vu, Mai The and Hong, Sung Kyung. *On the Sliding Mode Control Gain-Tuning: Novel Method and Experimental Verification* (2022). DOI 10.21203/rs.3.rs-1973402/v1. URL https://www.researchsquare.com/article/rs-1973402/v1.

[37] Bartoszewicz, Andrzej and Zuk, Justyna. "Sliding mode control x2014; Basic concepts and current trends." *2010 IEEE International Symposium on Industrial Electronics*: p. 3772–3777. 2010. IEEE, Bari, Italy. DOI 10.1109/ISIE.2010.5637990. URL http://ieeexplore.ieee.org/document/5637990/.

[38] Salas Gordoniz, Jorge Esteban. "Swinging Stabilization for an Underactuated blimp." (2022). URL https://www.youtube.com/watch?v=LA-f-ET_gmk.

[39] Kelly, Rafael, Santibáñez, Victor and Loría, Antonio. *Control of robot manipulators in joint space*. Advanced textbooks in control and signal processing, Springer, London [Heidelberg] (2005).

[40] Edgecombe, Gregory D. and Giribet, Gonzalo. "Evolutionary biology of centipedes (myriapoda: chilopoda)." *Annual Review of Entomology* Vol. 52 No. February (2007): pp. 151–170. DOI 10.1146/annurev.ento.52.110405.091326.

[41] Boase, Derek. "Online Adaptive Model-Free MIMO Control of Lighter-Than-Air Dirigible Airship." Ph.D. Thesis, University of Ottawa. 2024. URL http://ruor.uottawa.ca/handle/10393/45874. Publisher: Université d'Ottawa / University of Ottawa.